Fast, All-Optical Rayleigh Wave Microscope: Imaging on Isotropic and Anisotropic Materials

Matthew Clark, Steve D. Sharples, and Michael G. Somekh

***Abstract*—A fast, non-contact Rayleigh wave scanning microscope is demonstrated, which is capable of scan rates of up to a maximum of 1000 measurements/s with typical speeds in up to 250 measurements/s on real samples. The system uses a mode-locked, Q-switched Nd:YAG laser operating at a mode-locked frequency of 82 MHz and a Q-switch frequency of 1 kHz. The Q-switch frequency determines the upper limit of the scanning rate. The generating laser illumination is delivered and controlled by a computer-generated hologram (CGH). The generating laser produces around 30 pulses at 82 MHz and additional harmonics at 164 and 246 MHz and above. The microscope can operate at these harmonics provided the spatial bandwidth of the optics and the temporal bandwidth of the electronics are suitable. The ultrasound is detected with a specialized knife-edge detector.**

The microscope has been developed for imaging on isotropic materials. Despite this, the system can be used on anisotropic materials, but imaging and interpreting images can be difficult. The anisotropy and grain structure of the material can distort the Rayleigh wavefront, leading to signal loss. A model has been developed to simulate polycrystalline-anisotropic materials; this is discussed along with possible solutions that would overcome the problems associated with anisotropy.

Rayleigh wave amplitude images are demonstrated on silicon nitride at 82 and 164 MHz and on polycrystalline aluminium at 82 MHz.

I. Introduction

Laser ultrasound techniques [1] have many attractive properties, including non-contact, non-destructive, and remote measurement of material properties. However, most non-destructive laser ultrasound techniques are too slow to be useful for imaging.

We have built a fast-scanning Rayleigh wave microscope capable of scan speeds of up to 1000 measurements/s. The scanning speed is, at present, limited by the scan stages to a practical speed of up to 250 points/s. At lower speeds, averages of many measurements can be taken at each point. The system is very successful on both isotopic materials but less so on anisotropic materials where the anisotropy can distort the Rayleigh wavefront and cause signal loss.

In this paper imaging, is demonstrated on both isotopic and anisotropic materials. The problems with anisotropy have been studied and modeled, allowing the investigation of possible solutions. The model and simulations will be presented elsewhere. A simple change of the acoustic-optics is suggested to improve the signal on weakly anisotropic materials. However, an adaptive acoustics approach, similar to adaptive optics, is required to image on a wide variety of anisotropic materials.

Manuscript received December 15, 1998; accepted August 10, 1999.

The authors are with the Department of Electrical and Electronic Engineering, University of Nottingham, University Park, Nottingham NG7 2RD, UK (e-mail: eezmgs@een1.eee.nott.ac.uk).

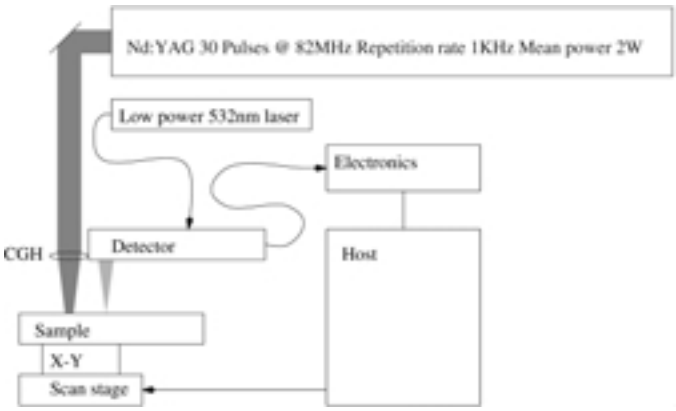

Fig. 1. Schematic diagram of experiment.

II. Experimental Setup

A mode-locked Q-switch Nd:YAG laser is used with a CGH to generate Rayleigh waves on a sample surface (Fig. 1). These are detected using a specialized knife-edge detector.

A. Generation

The generating laser has a mode-lock frequency of 82 MHz; it also produces harmonics of 82 MHz up to gigahertz frequencies. This laser is Q-switched at a frequency of 1 kHz to increase the peak power and reduce the mean power output. The Q-switch pulse is approximately 300 ns long, giving about 30 pulses at 82 MHz. The mean power output is approximately 2 W, giving each pulse approximately 60 μJ of energy and a peak power of approximately 300 kW.

The laser light is delivered to the sample surface by a CGH. This focuses and shapes the laser beam to produce a 60° arc of light (radius, 10 mm) on the sample surface. The binary phase CGH was designed using a direct-search method [2] and fabricated in quartz.

The use of a CGH to deliver and control the intensity distribution greatly simplifies the generation optics. The CGHs can be designed to produce near arbitrary intensity

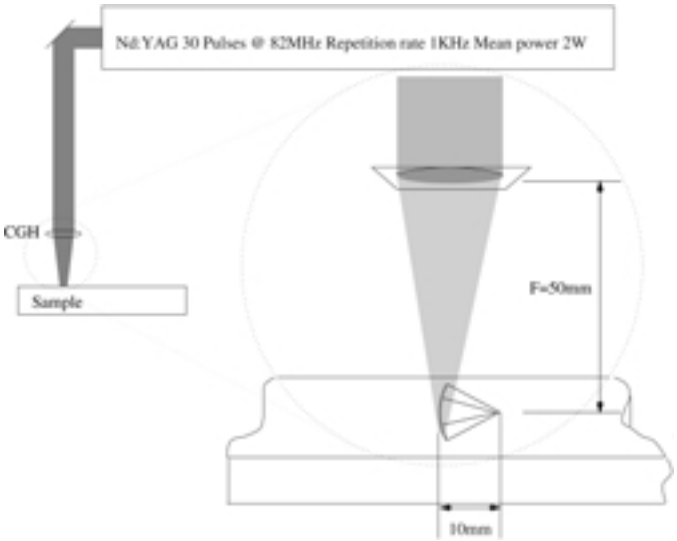

Fig. 2. Schematic diagram of generation optics.

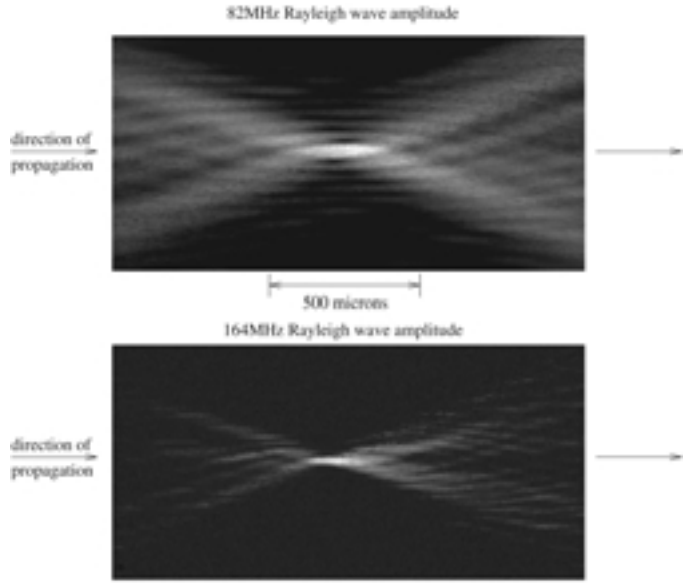

Fig. 3. Rayleigh wave amplitude measured around the center of an arc generation source. The sample was aluminium-coated glass ($v_{\text{Rayleigh}} \approx 3075$ ms^{-1}).

distributions over three dimensional as well as flat sample surfaces. The CGHs have also been fabricated to control the frequency [3] content of the generated ultrasound by illuminating the sample with multiple lines spaced to select the correct frequency.

The use of an arc generation source produces Rayleigh waves with a circular wave front, which propagate to a focus at the center of the arc (Fig. 2). The width of the focused Rayleigh wave can be estimated from the NA of the arc (≈ 0.5) and the wavelength of the focused Rayleigh wave. This system is similar (but non-contacting) to the surface wave microscope of Atalar and Koymen [4]. For a typical metal with a Rayleigh velocity of ≈ 3000 ms^{-1}, the wavelength at 82 MHz is ≈ 35 μm, which gives the width of the focal spot as ≈ 70 μm. The amplitude of the Rayleigh wave at the focus can be estimated using conservation of energy as approximately 10 times the amplitude, leaving the generating line at 82 MHz.

Fig. 3 shows the Rayleigh wave amplitude distributions around the center of an arc-generating source for 82 and 164 MHz. It can be seen that the size of the focus corresponds well to the expected size and that the size of the focus at 164 MHz is one-half of that of the 82-MHz signal.

B. Detection

The detector uses a knife-edge system, replacing the knife-edge with a split photo-diode (Fig. 4). As the Rayleigh wave passes under the probe, the reflected light is deviated, and this deviation is detected by the split diode. The AC signal is passed through a two-stage amplitude detection system. The first stage detects the amplitude of the high frequency signal with a forward biased diode; the second stage amplifies, detects, and extends the resultant low frequency signal with an unbiased diode, allowing the amplitude to be measured with an ordinary A-D system. This arrangement gives good linearity and removes the need for digital signal processing, which can be expensive and slow in comparison.

III. Imaging Results

Fig. 5 shows Rayleigh wave images of cracks resulting from a Vickers hardness test on a silicon nitride sample. These were taken at 82 and 164 MHz using this system at a scan rate of 40 pixels/s taking an average of 20 measurements at each point. The Rayleigh wave in these pictures was traveling from top to bottom. Distinctive fringes (pitch equal to one-half the Rayleigh wavelength, giving 35 and 17.5 μm, respectively) can be seen above the horizontal cracks, resulting from interference between the incoming wave and a wave reflected from the cracks [5]. The extent of the fringes is limited by the short Q-switch pulse length of the generating laser, which limits the length of the Rayleigh wave packet. The width of the fringes and shadow region is greater in the image taken at 164 MHz than the image taken at 82 MHz; this is thought to result from the cracks, which are reduced in depth toward their ends, allowing the 82-MHz signal to pass underneath.

With minor modification, this system can take velocity images. At present, this requires the waveforms to be captured on a digital oscilloscope, which reduces the scan rate to around one point/s. We are working on analog phase sensitive detectors that will allow us to perform fast simultaneous amplitude and velocity imaging.

IV. Imaging on Anisotropic and Polycrystalline Materials

The current system has been designed and optimized for imaging on isotropic materials. A key feature of this design is the long Rayleigh wave focal length of 10 mm that allows the light energy to be spread over a greater area, reducing peak intensity. With a Rayleigh wave focal length

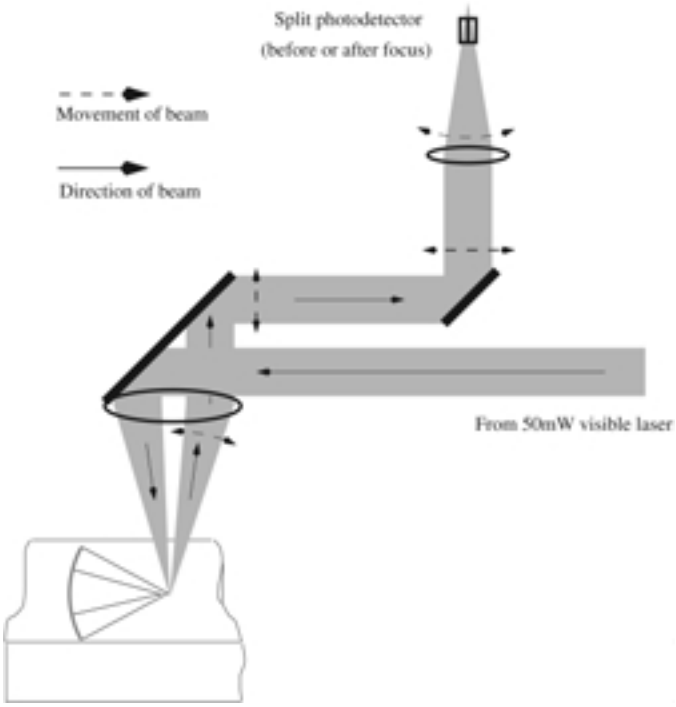

Fig. 4. Schematic diagram of detection optics.

of 10 mm, the light can be put into a single arc without any surface damage. At shorter focal lengths, multiple arcs are required to ensure non-destructive imaging.

This is not ideal for anisotropic materials because the wave can be scattered and distorted by the anisotropic grains that make up the material (Section IV, A). Shorter focal lengths are better suited to imaging on anisotropic materials because they result in less distortion and scattering (Section IV, C, 1). However, even this system can be used for imaging on weakly anisotropic materials with a large grain structure.

Fig. 6 and 7 show a SAW image taken on a piece of aluminium at 82 MHz. The aluminium sample had a slot milled into the back that was 1 mm wide and 30 mm long. This was at an angle of 1° to the top surface of the sample and broke the surface at one end. This provided a subsurface void with a depth variable from 0 to ≈ 300 μm. In Fig. 6 and 7, the SAW signal travels from top to bottom, and the slot runs horizontally across the images, breaking the surface on the right. Distinctive (high frequency) horizontal fringes can be seen in Fig. 6 about one-third of the way down the image. These are caused by the incoming SAW interfering with a wave reflected from the edge of the subsurface void. There are dark patches or speckles present at random positions across the image. These speckles are caused by the anisotropy and grain structure of the sample.

Fig. 7 contains three low resolution SAW images taken from the same area as that in Fig. 6. The difference between these images lies in the way the experiment was set up. Prior to scanning, the optical probe is moved relative to the generating arc to find the focus of the SAWs. In

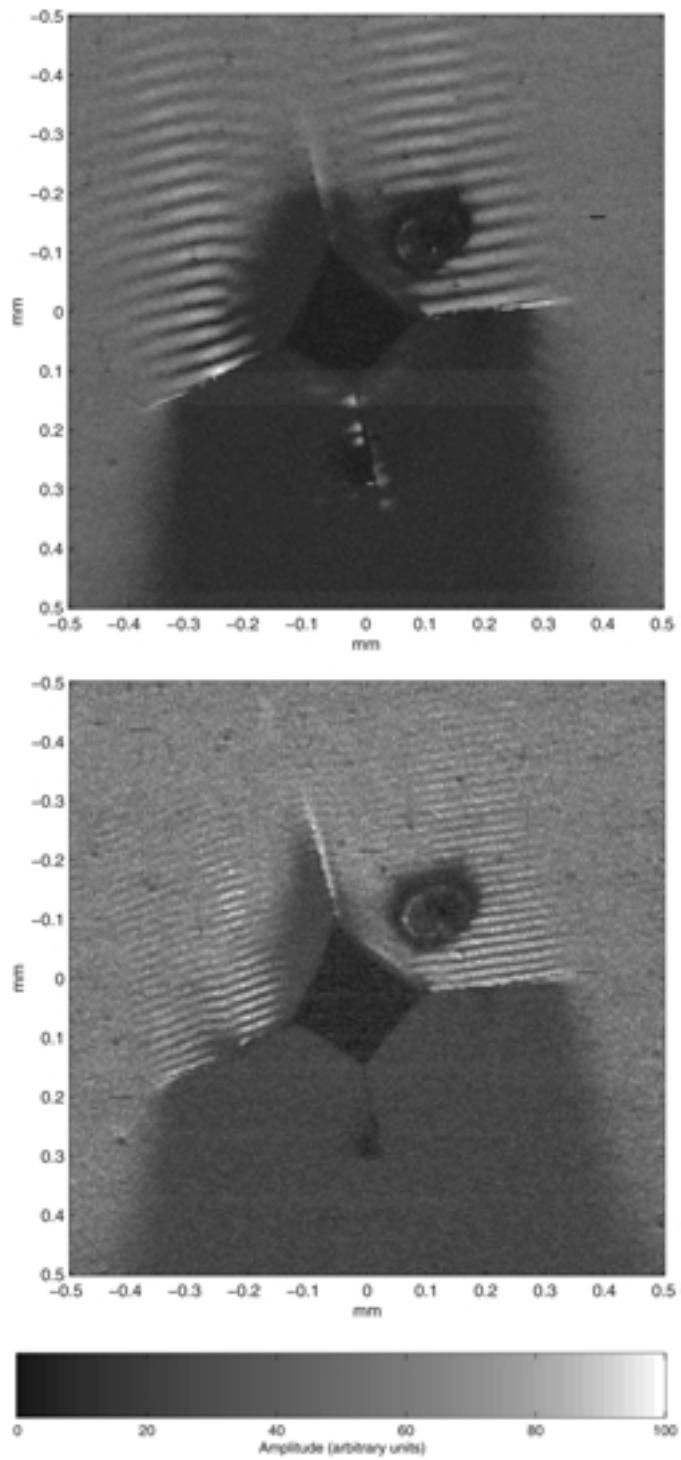

Fig. 5. Rayleigh wave amplitude image of cracks around a defect in silicon nitride. The upper image was taken at a frequency of 82 MHz, and the lower image was taken at 164 MHz. The image resolution was 5 μm in both directions. The circular dark patch (above and right of center) is caused by dust on the sample surface. The Rayleigh wavelengths were 70 and 35 μm, giving the reflected fringes wavelengths of 35 μ and 17.5 μm, respectively. Each image took approximately 20 min to scan in the 40 000 pixels required.

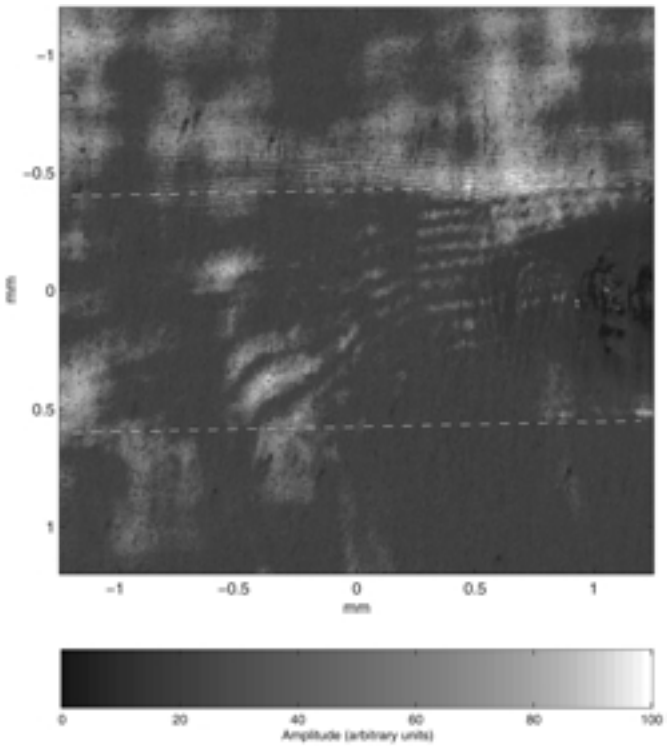

Fig. 6. SAW scan of a subsurface void in aluminium. In this image, characteristic interference fringes are seen at the edge of the void. The dashed lines mark the approximate position of the slit. The coarse fringes visible in the region of the slit are thought to be beat fringes caused by the propagation of different Lamb wave modes.

Fig. 6, the focus was found on a piece of glass prior to scanning; this was then replaced by the sample, and the scan was performed without additional adjustment. In Fig. 7, the probe was adjusted to find the focus of the SAWs at a different location on the sample for each image.

A. Image Speckle and "Static" Turbulence

All four images in Fig. 6 and 7 show a distinctive "cloudiness," which is associated with the focal position of the SAWs moving relative to the generating arc (and detection probe). This occurs because the anisotropy and grain structure of the metal sample aberrates the SAW wavefront as it travels through the sample, resulting in signal loss evident as the dark patches or speckles in Fig. 6 and 7.

By setting up the detection probe position using a glass (isotropic) sample (as for Fig. 6), we can ensure that the probe is at the geometric focus of the arc.

The anisotropy and grain structure of the samples can degrade the imaging ability of this system, reducing the signal level and producing dark speckles. This can make the images difficult to interpret. This restricts the system to isotropic and weakly anisotropic samples or single crystal anisotropic samples. In the subsequent subsections, techniques for overcoming this problem are suggested.

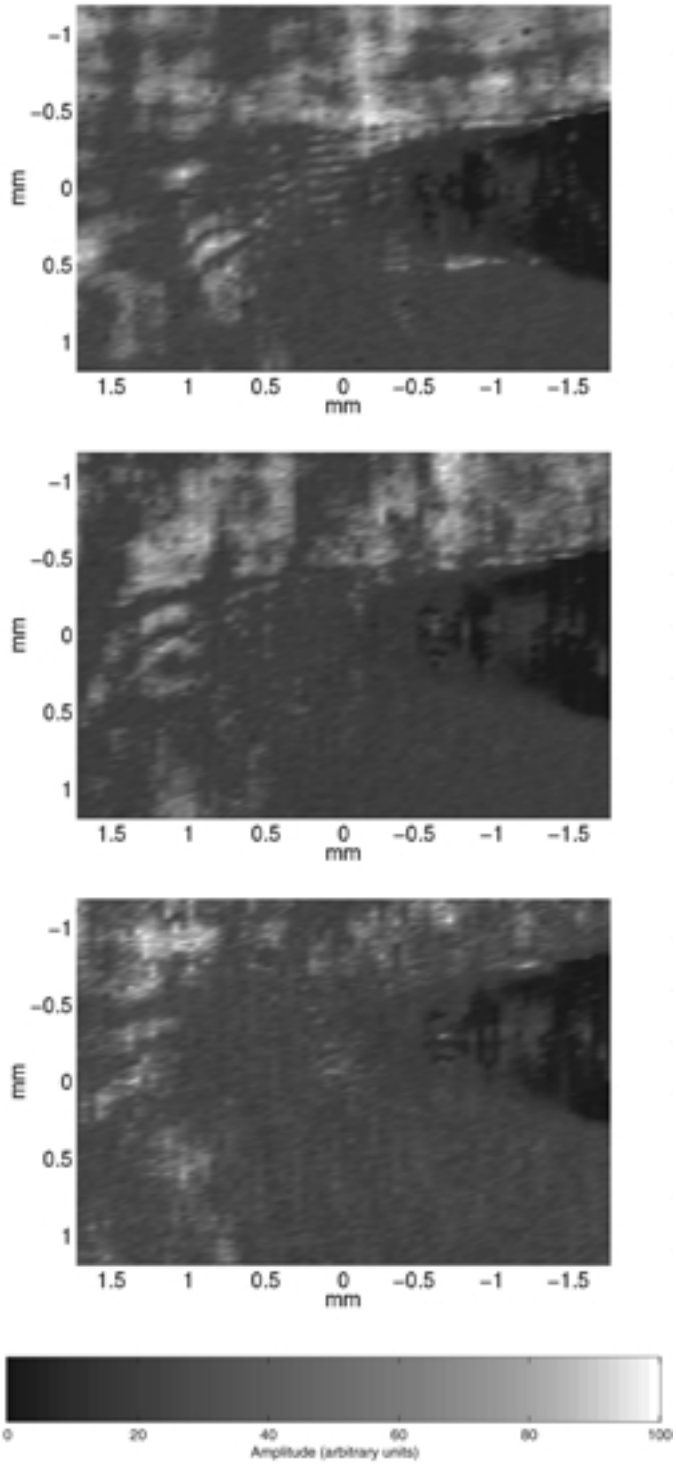

Fig. 7. SAW scans of a subsurface void in aluminium that demonstrate image speckle arising from the random orientation of the anisotropic metal grains.

1. Static Turbulence: The problem of trying to image SAWs through a polycrystalline anisotropic material is similar to the problem of optical imaging through a turbulent atmosphere [6]. A crucial difference is that the aberration caused by the polycrystalline anisotropic sample is fixed in time and only changes when the sample moves. The anisotropy may be thought of as introducing a "static" turbulence.

The aberration is introduced as the SAW travels through the grains that make up the sample. The grains are orientated randomly with respect to the propagation of the SAW. If the material is anisotropic, then the SAW velocity through the grain depends on its orientation. As different parts of the wavefront travel through different grains, the wavefront becomes aberrated and attenuated. Attenuation above the material absorption results from scattering and reflection of the SAW by the grain interfaces. The effect of the aberration depends strongly on the grain size, the degree of acoustic anisotropy, and the experimental set-up [7].

We identified three regimes where different effects dominate the propagation of the SAWs. These depend principally on the grain size and also the degree of anisotropy:

- Single crystal. This produces a "geometric" aberration and no scattering losses. The aberration can be calculated in advance, and a single "arc" corrected for the slowness surface of the sample is suitable for imaging.
- Large grains. The sample is made up of many grains with dimensions longer than the wavelength of the SAWs. This causes random aberration of the wavefront and moderate attenuation, although the principal cause of signal loss is the aberration. In this case, the signal may be recovered by using a corrected arc to compensate for the aberration, although different compensation is required for each scan position. This is similar to the problem of imaging through a turbulent atmosphere [6].
- Small grains. The sample is made up of grains with dimensions similar or smaller than the wavelength of the SAWs. This results in attenuation and scattering of the SAWs so that the focal position of the SAWs does not move substantially but is attenuated by the scattering. In this case, it is difficult to recover the signal unless the distance between the generation and detection points is reduced.

In all cases, the larger the anisotropy, the larger the aberration and greater the scattering. The scattering loss tends to be smaller than the signal loss caused by aberration, even for large anisotropies (Section IV, B, 1).

B. Simulation of Speckle

We use a phase screen method for simulating the propagation of SAWs through aberrating samples. The sample between the generation and detection planes is divided into a number of layers, the SAWs are propagated between the layers using an angular spectrum technique assuming a uniform average velocity. At the end of each layer, a phase (phase screen) is added to the SAW wavefront to account for the velocity variations in the material (Fig. 8). The phase screens are generated randomly using a model for the spatial distribution of the velocity variations. This model is at an early stage of development and mainly dependent on the material grain size. The path from the initial plane to the focal plane is divided up into a sufficient number of layers (and screens) to ensure the screens are "weak" and that the spatial variation of the screens adequately represents the grain size [8].

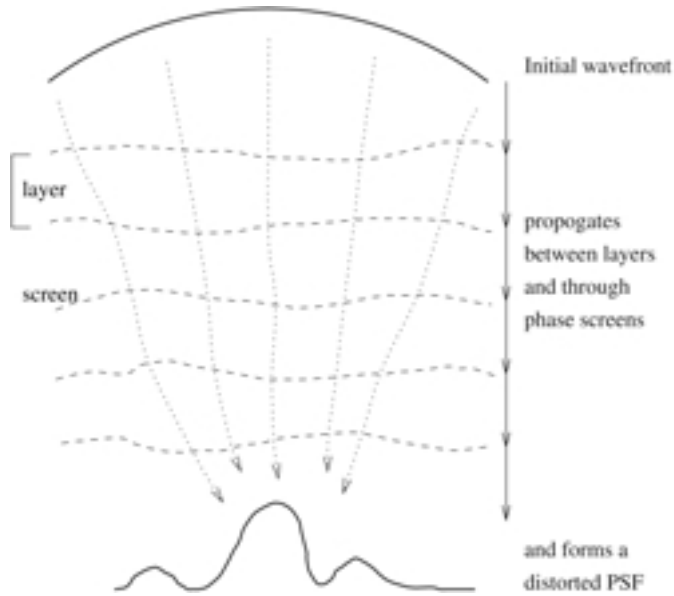

Fig. 8. The simulations are carried out by propagating the wave between layers where a random phase screen is added to the wavefront.

To simulate the effect of scanning, the phase screens are generated in advance, and the wavefront position is moved with respect to the screens. When the layer thickness is greater than the distance between adjacent scan points, fractions of screens are used with appropriate variation of the screen strength. This model allows simulations to be performed for a wide range of generation and detection schemes and a wide range of grain sizes and degrees of anisotropy.

1. The Effect of Scattering: The phase screen model does not take the attenuation caused by reflections at grain interfaces into account. This can be roughly estimated by calculating an average total attenuation for all of the layers from the estimated mean power reflection coefficient for each layer, R. The fraction of the SAW power, T, reaching the focal line can be estimated as $T \sim (1-R)^N$, where N is the number of layers and $R \sim \left[\frac{1}{2}\delta c/(2+\delta c)\right]^2$ where δc is the degree of anisotropy or the fractional change in velocity between the slowest and fastest directions of the material.[1] Although this is not strictly correct for SAWs, it is consistent with experimental results for reflections at

[1]This assumes that the mean velocity change is approximately $\frac{1}{2}\delta c$.

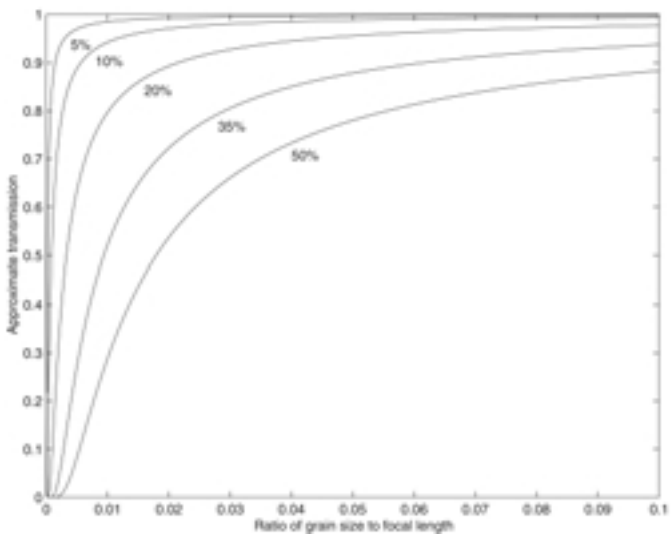

Fig. 9. Estimated SAW transmission versus the ratio of the grain size to the focal length and degree of anisotropy.

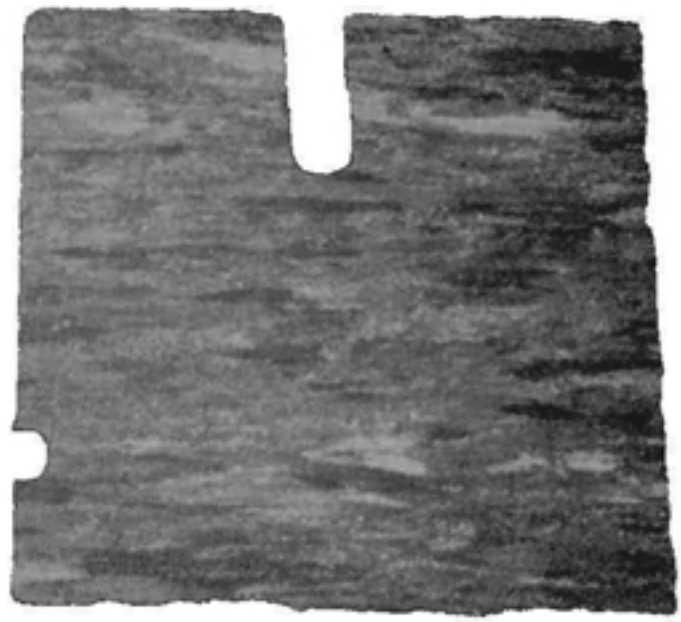

Fig. 10. Photography of the surface of a subsection of the aluminium sample used in Fig. 7 and 12. The surface has been etched to show the macroscopic grain structure that is dominated by long, thin grains, presumably formed by rolling. At higher magnifications, other etches revealed a very small number of smaller grains ($\approx$ 20 μm) found mainly at the boundaries of the large grains. This was typical of presumed rolled samples. Cast aluminium samples were found to be entirely made up of small grains ($\approx$ 20 μm).

grain boundaries observed with scanning acoustic microscopes [9].

This simple model assumes that the grain size is greater than the wavelength and that scattering only occurs as a result of Rayleigh wave reflections at grain boundaries.

Fig. 9 shows the transmission coefficient for SAWs versus the ratio of the grain size to the focal length for various degrees of anisotropy. This shows that, provided that the ratio of the grain size to the Rayleigh wave focal length is not very small, the attenuation caused by scattering is low, even for large anisotropies. Thus, the main cause of signal loss for larger grain sizes is the speckle caused by the aberration rather than scattering.

2. Simulation of Fig. 6: The grain size of the samples used in Fig. 6 and 7 was measured optically after etching the surface. Fig. 10 shows a photograph of part of the etched sample surface. The sample was found to be made mainly of large elongated grains, approximately 1000 μm long and 250 μm wide. This structure results from rolling, and the long direction of the grains lies along the rolling direction. By measuring the number of boundary crossing per unit length over a range of angles, an effective grain size of 625 μm in the long direction and 260 μm in the short direction was determined for use in the model.

Fig. 11 shows the simulated SAW point spread function across the focal line as the scan position is moved using the measured effective grain size. This simulation was performed with the propagation along the short axis of the grains. It can be observed that the point spread function is distorted and moves around and, in some places, breaks up altogether. When scanning on a sample, the optical probe measures the SAW amplitude at one point only. Assuming this point is fixed with respect to the generation, the position of the SAW point spread function will move relative to the detection point, causing the signal strength to drop. The distortion is more severe when propagating along the long direction of the grains because the phase screens are stronger and contain higher spatial frequencies.

Fig. 12 shows measured and simulated scans on this sample; the direction of propagation of the SAWs is orientated with either the long direction or short direction of the grains. The images on the left are taken with the SAW propagating along the rolling direction; those on the right are taken with the SAW propagating across the rolling direction. The top row shows real SAW images taken on a blank aluminium sample. The middle row shows simulations using the same grain sizes and direction. The bottom row shows the same simulations but using tilt correction (Section IV, C, 2). The real images differ from the simulations as we have no practical way of determining the particular orientation of the grains in the sample, but it can be seen that the distribution of speckles in the simulated images is similar to that of the measured images.

The current model for generating phase screens is very simple. Further work on phase screens and speckle statistics could improve the quality of these simulations.

C. Recovering the Signal

It is clear that to produce good, easy-to-interpret SAW images on a wide variety of anisotropic materials, methods of recovering the SAW signal must be found. We have, using the model developed (Section IV, B), investigated the effect of the static turbulence and some solutions.

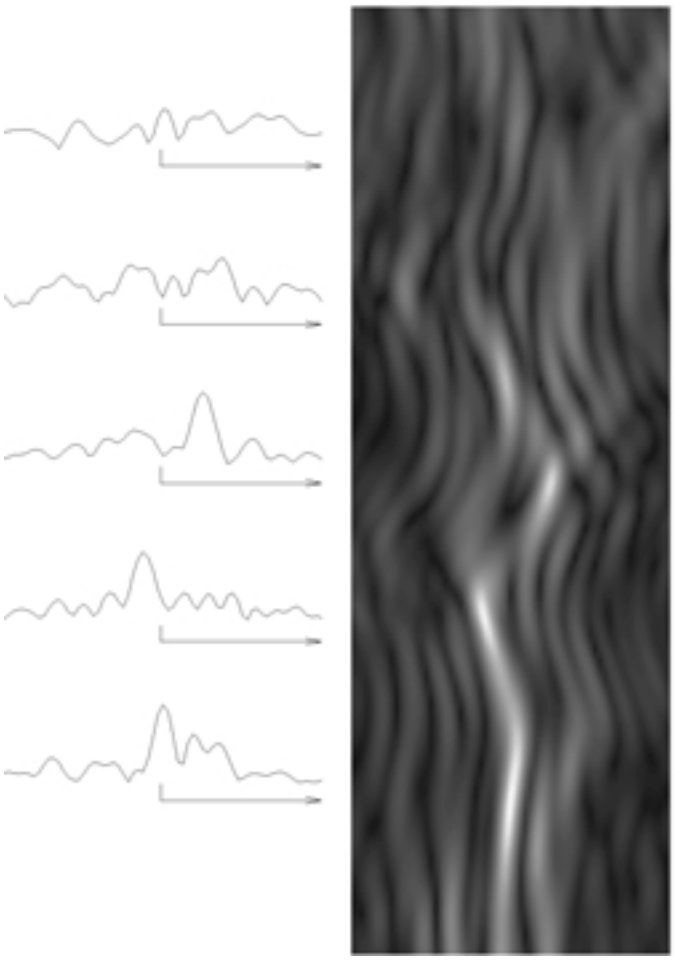

Fig. 11. Simulation of the SAW point spread function (PSF) as the sample position is moved. The SAW PSF is plotted horizontally, and the scan position is plotted vertically. The PSF can be seen to "wander" about as the sample position is moved. If the optical probe is placed in a fixed position, the SAW signal will change in strength as the PSF moves under it. This is responsible for the "cloudiness" observed in Fig. 6 and 7.

1. Simple Improvements: An obvious way of reducing both the attenuation and aberration of the SAW is to shorten the focal length of the generating arc. At the current radius of 10 mm, the generating laser does not ablate the sample surfaces. At smaller radii, the optical intensity would have to increase to maintain the same signal level that would result in destructive surface ablation. This could be counteracted by using multiple arcs spaced by the required wavelength. In this system, a generating source of 16 lines could be accommodated without reducing the signal bandwidth. This would allow the use of a generating source with a mean SAW focal length of 2 mm. At focal lengths shorter than this, the heating caused by the generating source may perturb the measurements at the focus.

The use of a large number of multiple lines means that the generating source has a limited bandwidth and that the arc separation must be matched to the material velocity. This can be done by tailoring the CGH design to the material velocity or using a simple optical zoom system to adjust the line spacing.

Fig. 13 shows simulations of SAW signals on aluminium with the same grain size as Fig. 12 but with a SAW focal length of 2 mm.

2. Adaptive Optics/Acoustics: In the first two regimes mentioned previously, an adaptive optics [6] approach may be used to recover much of the signal lost through aberration.

The images shown in Fig. 13 without tilt correction show a marked improvement over those shown in Fig. 12, but they are not perfect. It can be seen that, although the signal loss is not as frequent as in Fig. 7 and that scans over an area of 3 mm^2 could be accomplished without significant signal loss, there is considerable room for improvement. Examination of the SAW point spread function in the regions where the signal drops reveals that the point spread function is largely intact but has moved sideways, out of the detection region. The signal may be retrieved in these areas using a low order "adaptive-acoustics" system, where the shape of the generating arc(s) are changed to bring the signal back to the correct position. The simplest form of correction is "tilt" correction, where the shape of the generating profile is not changed but simply angled or tilted to steer the acoustic signal back to the detection point.

It is evident from Fig. 12 and 13 that considerable correction could be achieved in these cases by using tilt correction only. This can be easily implemented into our current system by tilting the generating CGH (thus tilting the arc). The amount of tilt required is relatively small; the corrections shown in Fig. 12 and 13 would require the CGH to be tilted by a few degrees.

3. Wavefront Sensing: A major problem for this approach is determining what correction (tilt or higher order) to apply. It is possible to sense the wavefront by scanning the optical probe along the focal line and measuring the amplitude and phase, but this is very slow in comparison with the scan speed. We are developing a linear array of SAW detectors for SAW wavefront sensing.

In the short term, an iterative optimization approach based on the CGH design algorithm may work because the aberration is static and slowly changing. This would work by adjusting the tilt slowly as the scan progressed to maximize the signal; the tilt angles would be stored and reoptimized at each scan line.

Higher order correction would improve the signal further, but this would require some sort of wavefront sensing and more sophisticated control of the generating source.

4. Wavefront Correction: As mentioned previously, tilt correction may be achieved by tilting the CGH and, therefore, the generating arc. As the arc is tilted, the paths through the static turbulence will change but only very slightly as the range of required tilt angles is very small.

To provide higher order wavefront corrections, the arc will not only have to tilt but bend as well. This may be achieved by using a spatial light modulator (SLM) to

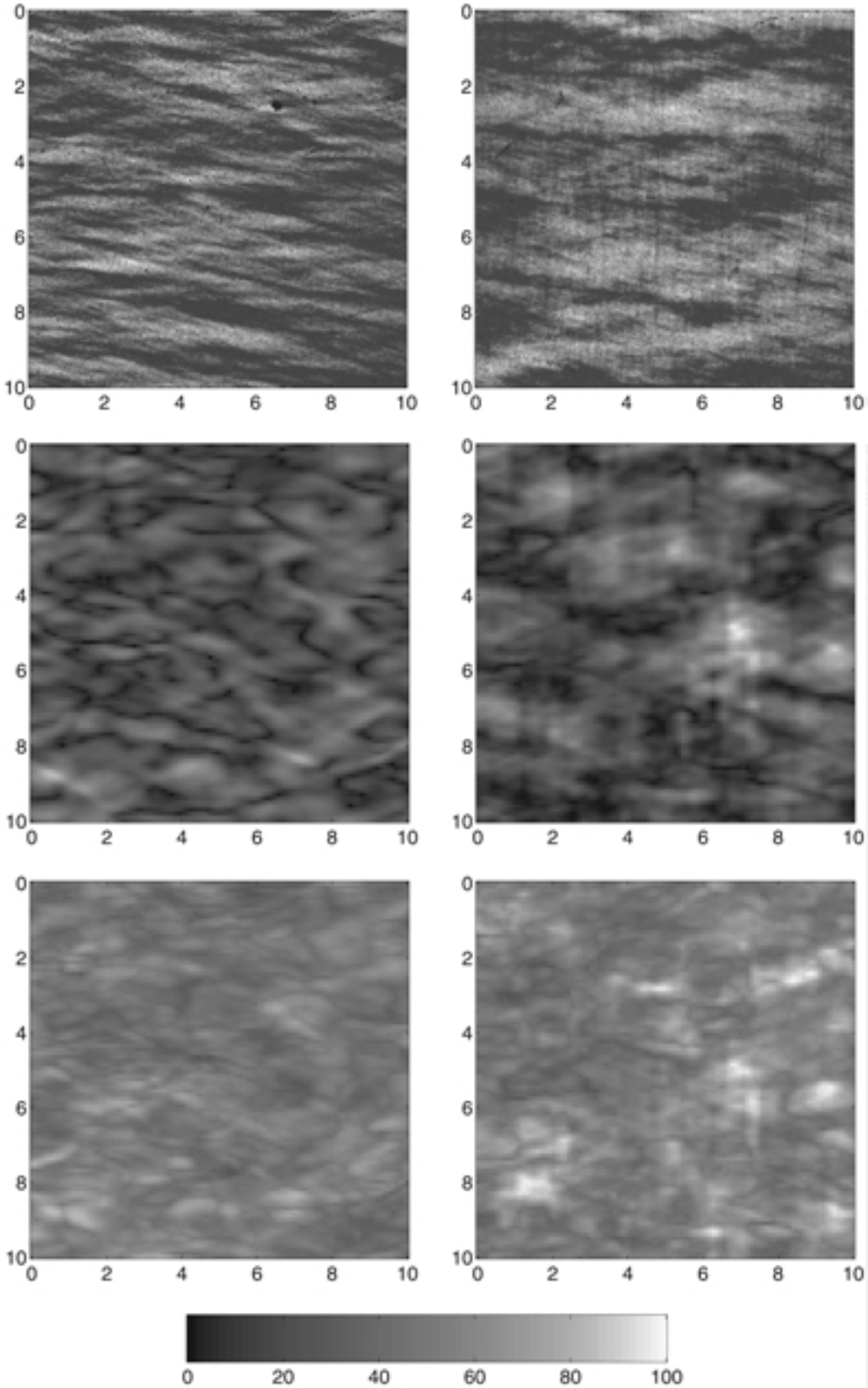

Fig. 12. Measured and simulated SAW amplitude on rolled aluminium (grain size $\approx 600 \times 250\ \mu$) using a SAW focal length of 10 mm. The left column shows results taken with the direction of propagation along the long axis of the crystals. The right column shows results taken with the direction of propagation along the short axis. The top row shows actual SAW amplitude measured on a blank sample, the middle row shows simulated SAW amplitude, and the bottom row shows simulated SAW amplitude using tilt correction. The measured images show additional (very fine) optical speckle not present in the simulations.

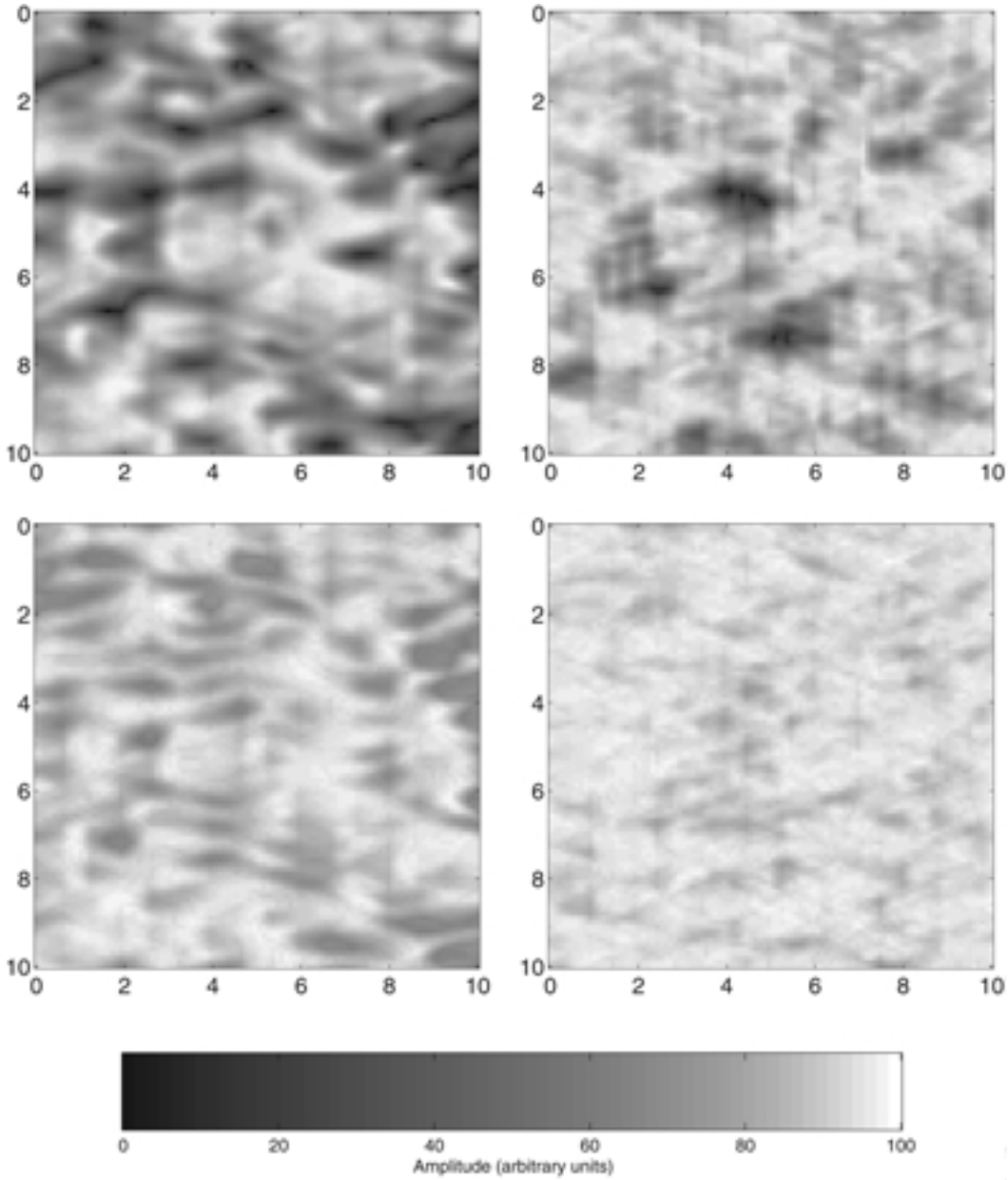

Fig. 13. Simulated SAW signals on aluminium for a SAW focal length of 2 mm. On the left, the direction of propagation is along the long axis of the crystals; on the right, it is along the short direction. The upper images are uncorrected, and the lower images have tilt correction.

form the hologram completely or work with a predesigned diffractive optical element (DOE) to correct the arc or form an image of the corrected arc, which can be projected onto the sample. Using a SLM to form the complete hologram is optically simple but has some significant drawbacks. The CGHs in current use are made up of four million pixels, SLMs of this resolution are not readily available, and the CGH design algorithm, which is required to get good performance from binary holograms, is too slow to work "on the fly" during scanning. The use of an SLM in conjunction with a DOE is an attractive compromise, where the DOE performs the image (arc) formation and a low resolution SLM is used to change the optical wavefront moving the arc. Designing the correct low resolution pattern for the SLM would be easy to achieve at current scan rates. Perhaps the most attractive scheme is the use of an SLM as an imaging device. This would involve the SLM displaying the required generation distribution, which could then be projected onto the sample surface.

V. Conclusion and Further Work

This paper has reported a new SAW scanning microscope. This uses optical generation and detection and is noncontacting. The microscope uses a CGH to deliver and control the generating laser beam, and, as a result, we can achieve good detection signal levels without any surface damage. This allows us to use analogue electronic amplitude detectors and suggests that we can take measurements at the full repetition rate of the generating laser

(currently 1 kHz). Presently, the scan rate of the microscope is limited to 250 points/s by the scan stages. The ability of this microscope to image surface and near surface cracks and voids has been demonstrated on silicon nitride and aluminium.

This technique is useful in its present form as an imaging tool for the inspection of isotropic materials. On anisotropic materials, the anisotropy can degrade the signal and make the images difficult to interpret.

The effect of the anisotropy is to aberrate the SAW wavefront. We have developed a model allowing us to simulate this effect and propose that an "adaptive acoustic" technique may be used to overcome this limitation in the same ways that adaptive optical techniques can be used to remove the effect of atmospheric turbulence on telescope images. In the first instance, we have shown that shortening the SAW focal length and using a simple tilt system may be used to recover much of the SAW signal. In some instances, this may be done without a SAW wavefront sensor.

We intend to implement these adaptive acoustics approach shortly and are developing novel techniques for wavefront sensing and adaptive generation of SAWs to make higher order wavefront corrections.

References

[1] C. B. Scruby and L. E. Drain, *Laser Ultrasonics, Techniques and Applications*. Bristol, UK: Adam Hilger, 1990.

[2] M. Clark and R. Smith, "A direct-search method for the computer design of holograms," *Opt. Commun.*, vol. 124, no. 1–2, pp. 150–164, 1996.

[3] M. Clark, F. Linnane, S. D. Sharples, and M. G. Somekh, "Frequency control in laser ultrasound with computer generated holography," *Appl. Phys. Lett.*, vol. 72, no. 16, pp. 1963–1965, 1998.

[4] A. Atalar and H. Koymen, "Use of a conical axicon as a surface acoustic-wave focussing device," *IEEE Trans. Ultrason., Ferroelect., Freq. Contr.*, vol. 34, no. 11, pp. 53–63, 1987.

[5] K. Yamanaka and Y. Enomoto, "Observation of surface cracks with the scanning acoustic microscope," *J. Appl. Phys.*, no. 2, pp. 846–850, 1982.

[6] R. K. Tyson, *Principles of Adaptive Optics*. Chestnut Hill, MA: Academic Press, 1991.

[7] M. G. Somekh, G.A.D. Briggs, and C. Ilett, "The effect of elastic-anisotropy on contrast in the scanning acoustic microscope," *Philos. Mag. A*, vol. 49, no. 2, pp. 179–204, 1984.

[8] M. D. Fisk and G. D. McCartor, "The phase screen method for vector elastic waves," *J. Geophys. Res.*, vol. 96, no. B4, pp. 5985–6010, 1991.

[9] M. G. Somekh, H. L. Bertoni, G.A.D. Briggs, and N. J. Burton, "A two-dimensional imaging theory of surface discontinuities with the scanning acoustic microscope," *Proc. R. Soc. Lond. A*, vol. 401, no. 1820, pp. 29–51, 1985.

Matthew Clark was born in Norwich, UK, in 1968. His first degree was in Physics from Manchester University, UK, where he graduated in 1990. He went to Imperial College, London, as a research assistant and stayed to complete his PhD in optics in the Physics Department in 1997. He has worked in the School of Electrical and Electronic Engineering, University of Nottingham, since 1996.

Steve D. Sharples was born in Preston, UK, in 1975. He graduated with a Masters of Engineering degree in Electronic Engineering from the University of Nottingham in 1997 and is currently in his third year of his PhD, researching surface acoustic waves and laser ultrasound.

Michael G. Somekh was born in Manchester, UK. His first degree was in Metallurgy and the Science of Materials from Oxford University, where he graduated in 1976. He completed his PhD in Microwave Electronics in the Physics Department of Lancaster University. In 1981, he returned to Oxford as a postdoctoral research assistant and later SERC research fellow. In 1985, he joined University College London as a lecturer and left in 1989 to go to the School of Electrical and Electronic Engineering, University of Nottingham, where he has established the optical engineering activity. His research involves the application of optical engineering to industrial measurement, surface profiling, microscopy and laser ultrasound. Since 1995, he has held the position of Professor of Optical Engineering.